2010 IEEE International Conference on Robotics and Automation
Anchorage Convention District
May 3-8, 2010, Anchorage, Alaska, USA

Simulation and Experimental Studies on Passive-dynamic Walker That Consists of Two Identical Crossed Frames

Fumihiko Asano

Abstract— **This paper proposes a novel spoke-like passive-dynamic walker that consists of two identical crossed frames whose center of mass is positioned on the central axis. The purpose of this study is to develop an easy test-bed for investigating the roles of double-support phase and swing-leg retraction in limit cycle walking. The crossed frame as a swing leg does not have inherent rotational dynamics, and it rotates only in the presence of viscous friction at the central axis. We first analyze the properties of this walker through mathematical modeling. Next, we numerically investigate the gait efficiency, and discuss the effect of inertia moment and mass distribution of the crossed frame. Finally, we briefly report our experimental results.**

I. INTRODUCTION

Limit cycle walkers based on passive dynamics are good examples for efficient legged locomotion [1][2][3]. Their walking motion is energy-efficient and human-like, but there are still many differences between robotic walking and human walking. One of the most significant differences is existence of double-support phase. In limit cycle walking, the stance leg is instantaneously exchanged if the heel strike collision model is inelastic. In dynamic walking of humans and biped humanoids controlled based on zero moment point (ZMP), double-support phase plays an important role in stabilization of the gait generation. Also in limit cycle walking, the effect of double-support phase control must be effective to improve its stability and robustness.

The author has developed a novel spoke-like passive-dynamic walking machine shown in Fig. 1 to investigate the effects of double-support phase and swing-leg retraction [4][5][6][7][8] on the gait efficiency and stability. This machine appears something like an rimless wheel [9], but is a dynamic bipedal walker whose swinging motion is emerged by the viscosity. By taking the special configuration, we can conduct experimental study very easily without concerning the foot scuffing at mid-stance. We have a prediction that this walker would exhibit passive-dynamic walking incorporating double-support phase and exchange the stance leg more smoothly if the leg frame has elastic elements.

As mentioned, the primary goal of this study is investigation how double-support phase affects the properties of passive-dynamic gait, but this walker also has several interesting and meaningful properties as follows. This machine consists of two symmetric crossed frames whose center of mass (CoM) is positioned on the central axis. In other words, each leg has own counterweight and does not have the rotational dynamics. The swinging motion therefore does not emerge during stance phases in the absence of viscous friction. It is an interesting topic to investigate how the walking motion changes with respect to the friction and in what condition it converges to a stable limit cycle.

F. Asano is with the School of Information Science, Japan Advanced Institute of Science and Technology, 1-1 Asahidai, Nomi, Ishikawa 923-1292, Japan fasano@jaist.ac.jp

Fig. 1. Spoke-like passive-dynamic walker that consists of two identical crossed frames

Another goal of this study is to develop an efficient and robust locomotion system that can walk on uneven surface and can climb up a steep slope at high speed. Spoke-like locomotion machines are expected to achieve high adaptability to complex outside-environment [10]. Although this paper does not report, we are now considering to add a telescopic actuation reported in [11].

Although we have not investigated the passive-dynamic gait with double-support phases yet, several interesting results have been obtained through inelastic collision model corresponding to the walker shown in Fig. 1. This paper then reports the results; the mathematical modeling, the simulation results and the experiment of passive-dynamic walking on a treadmill.

II. OVERVIEW

The dynamic walker does not have any actuators and consists of two identical crossed frames as shown in Fig. 1. The blue leg frames are attached to the outer axis-frame, whereas the aqua leg frames are attached to the inner axis-frame. These two wheels can rotate independently around

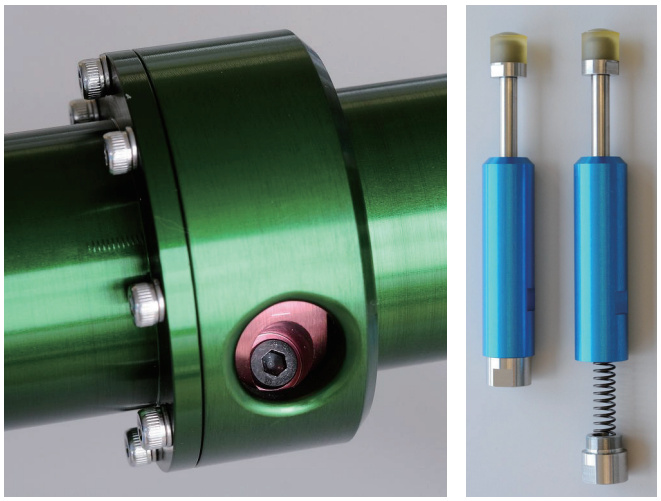

Fig. 2. Adjust screw for hip damper (left) and telescopic leg frame and its spring for running (right)

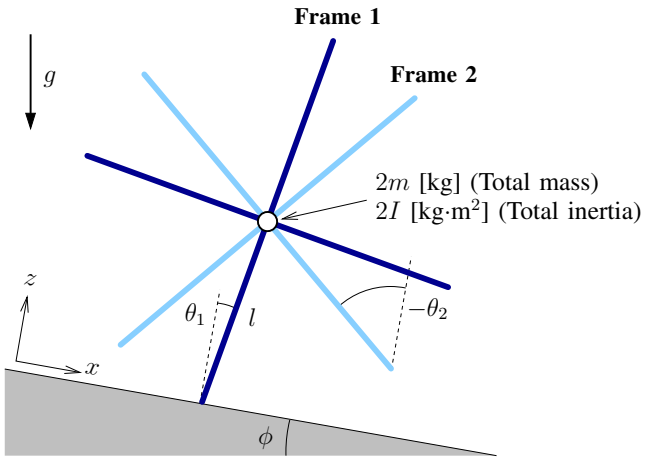

Fig. 3. Model of passive-dynamic walker that consists of two identical crossed frames

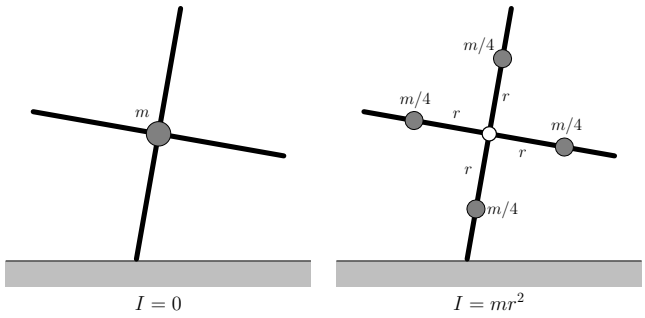

Fig. 4. Difference of inertia moment

the central axis, however, the viscous friction between them can be changed by the adjust screw shown in Fig. 2 left. End of each leg has a rubber for shock absorbing. Although we do not describe the detail, this walker is also able to run by replacing the leg frames with telescopic leg frames incorporating a spring as shown in Fig. 2 right. This would create double-support phase in passive-dynamic gait.

In this machine, each leg has own counterweight on its frame. The CoM of each leg is thus positioned on the hip joint, which is the same as the robot's total CoM. Therefore, the swing leg does not have its inherent dynamics for swinging. In this paper, we investigate the properties of this machine through modeling and mathematical analysis, and numerically investigate the effects of mass distribution and the inertial moment on the generated gait.

In a rimless wheel, it is obvious that the generated gait converges to a stable one-period limit cycle [12]. In this dynamic walker, however, it is not clear whether or not the generated gait is asymptotically stable or single period. It is far from impossible that the limit cycle becomes multiple period [2][3]. The subsequent sections report the basic results.

III. MODELING

A. Dynamic Equation

Fig. 3 shows the model of our dynamic walker and its coordinate system. Let θ_i [rad] be the angles of the frames with respect to vertical. Let m [kg] and I [kg·m^2] be the mass and inertia moment of each frame.

The kinetic and potential energies are given by

$$K = ml^2\dot{\theta}_1^2 + \frac{1}{2}I\dot{\theta}_1^2 + \frac{1}{2}I\dot{\theta}_2^2, \quad (1)$$

$$P = 2mgl\cos(\theta_1 + \phi), \quad (2)$$

where $g = 9.81$ [m/s^2] is the gravity acceleration.

One of the most important problems we discuss in this study is the effect of inertia moment. Fig. 4 shows the mass distribution of the crossed frame. The total mass and CoM position are identical in both cases, but the inertia moment is different. In the right case, the inertia moment is $I = mr^2 (= 4 \times \frac{mr^2}{4})$ [kg·m^2].

The viscous friction force at the central axis is given by $-\eta\left(\dot{\theta}_1 - \dot{\theta}_2\right)$ where η is the coefficient of viscosity and is positive constant.

The stance phase dynamic equation then becomes

$$\begin{bmatrix} I + 2ml^2 & 0 \\ 0 & I \end{bmatrix}\begin{bmatrix} \ddot{\theta}_1 \\ \ddot{\theta}_2 \end{bmatrix} + \begin{bmatrix} -2mgl\sin(\theta_1 + \phi) \\ 0 \end{bmatrix} = -\begin{bmatrix} 1 \\ -1 \end{bmatrix}\eta\left(\dot{\theta}_1 - \dot{\theta}_2\right). \quad (3)$$

We denote this as

$$\boldsymbol{M}\ddot{\boldsymbol{\theta}} + \boldsymbol{g}(\boldsymbol{\theta}, \phi) = \boldsymbol{S}u_H, \quad (4)$$

where the control input $u_H = -\eta\left(\dot{\theta}_1 - \dot{\theta}_2\right)$ represents the viscous friction force. The total mechanical energy is $E = K + P$ and its time derivative satisfies the relation $\dot{E} = \dot{\boldsymbol{\theta}}^{\mathrm{T}}\boldsymbol{S}u_H = -\eta\left(\dot{\theta}_1 - \dot{\theta}_2\right)^2 \leq 0$. The total mechanical energy thus decreases monotonically during stance phases. The swing leg rotates or the swing-leg's angular velocity changes only in the presence of viscous friction.

B. Transition Equations

Fig. 5 shows the configuration at heel strike. In this figure, the stance leg is exchanged from Frame 1 to Frame 2. From the geometrical relation, we can derive the angular positions

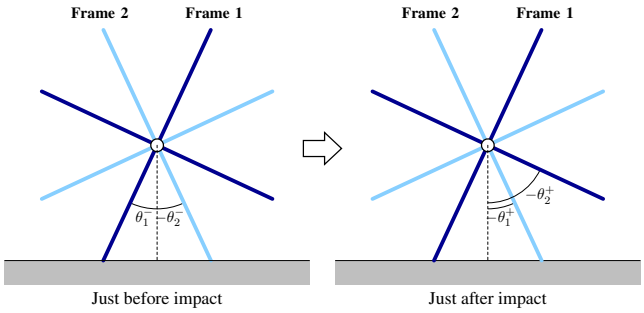

Fig. 5. Configuration at heel strike

as

$$\theta_1^+ = \theta_2^-, \tag{5}$$
$$\theta_2^+ = \theta_1^- - \frac{\pi}{2}, \tag{6}$$

where the superscripts "−" and "+" denote just before and just after impact. Here, we define the half inter-leg angle at impact, α [rad], as

$$\alpha := \frac{\theta_1^- - \theta_2^-}{2} = \frac{\theta_2^+ - \theta_1^+}{2} + \frac{\pi}{4} > 0. \tag{7}$$

We introduce an extended coordinate to the system to derive the impact dynamics. Let $\boldsymbol{q}_i = \left[\begin{array}{ccc} x_i & z_i & \theta_i \end{array}\right]^{\mathrm{T}}$ be the extended coordinate vector for Frame i $(i = 1, 2)$. The inelastic model for heel strike then becomes

$$\bar{\boldsymbol{M}}(\boldsymbol{q})\dot{\boldsymbol{q}}^+ = \bar{\boldsymbol{M}}(\boldsymbol{q})\dot{\boldsymbol{q}}^- - \boldsymbol{J}_I(\boldsymbol{q})^{\mathrm{T}}\boldsymbol{\lambda}_I, \tag{8}$$
$$\boldsymbol{J}_I(\boldsymbol{q})\dot{\boldsymbol{q}}^+ = \boldsymbol{0}_{4\times 1}, \tag{9}$$

where $\boldsymbol{q} = \boldsymbol{q}^- = \boldsymbol{q}^+$ and

$$\boldsymbol{q} = \left[\begin{array}{cc} \boldsymbol{q}_1^{\mathrm{T}} & \boldsymbol{q}_2^{\mathrm{T}} \end{array}\right]^{\mathrm{T}}, \tag{10}$$
$$\bar{\boldsymbol{M}}(\boldsymbol{q}) = \left[\begin{array}{cc} \boldsymbol{M}_1(\boldsymbol{q}_1) & \boldsymbol{0}_{2\times 2} \\ \boldsymbol{0}_{2\times 2} & \boldsymbol{M}_2(\boldsymbol{q}_2) \end{array}\right], \tag{11}$$
$$\boldsymbol{M}_i(\boldsymbol{q}_i) = \left[\begin{array}{ccc} m & 0 & ml\cos\theta_i \\ 0 & m & -ml\sin\theta_i \\ ml\cos\theta_i & -ml\sin\theta_i & I + ml^2 \end{array}\right], \tag{12}$$
$$\boldsymbol{J}_I(\boldsymbol{q}) = \left[\begin{array}{cccccc} 1 & 0 & l\cos\theta_1 & -1 & 0 & -l\cos\theta_2 \\ 0 & 1 & -l\sin\theta_1 & 0 & -1 & l\sin\theta_2 \\ 0 & 0 & 0 & 1 & 0 & 0 \\ 0 & 0 & 0 & 0 & 1 & 0 \end{array}\right]. \tag{13}$$

The relation between angular velocities just before impact and just after impact is given by

$$\dot{\boldsymbol{\theta}}^+ = \boldsymbol{\Xi}\dot{\boldsymbol{\theta}}^-, \tag{14}$$

where $\boldsymbol{\Xi} = \boldsymbol{\Xi}(\alpha) \in \mathbb{R}^{2\times 2}$ is detailed as

$$\boldsymbol{\Xi} = \left[\begin{array}{cc} \frac{2ml^2\cos(2\alpha)}{I+2ml^2} & \frac{I}{I+2ml^2} \\ 1 & 0 \end{array}\right]. \tag{15}$$

In addition, the following limit value

$$\lim_{I\to+0} \boldsymbol{\Xi} = \left[\begin{array}{cc} \cos(2\alpha) & 0 \\ 1 & 0 \end{array}\right] \tag{16}$$

is identical with the case of the simplest walking model [13]. The effect of the swing-leg motion just before impact vanishes in this case. As shown in Fig. 4, in real machines, the inertia moment always exists and its effect cannot be neglected. It is also main subject of this paper to investigate its effect on the gait efficiency. We numerically analyze it by changing the radius, r.

IV. ANALYSIS

This section analyzes the effects of mass distribution and swing-leg retraction (SLR) on the heel-strike collision from the energy-loss coefficient point of view, and numerically investigates the gait efficiency with respect to the inertia moment and slope.

A. Typical Gait

We first conducted numerical simulations to confirm that a stable limit cycle is generated in the presence of viscous friction.

Fig. 6 shows the simulation results where the slope is 0.50 [rad], $r = 0.30$ [m] and $\eta = 0$ [N·m·s/rad]. In this case, the swing leg does not have rotational force. Fig. 6 (a) and (b) show that the swing leg maintains its angle with respect to vertical and does not rotate during stance phases. The half inter-leg angle at impact converges to $\alpha = \pi/2$ [rad] in this case. Fig. 6 (c) also shows that the total mechanical energy is kept constant during stance phases and it converges to the steady value. It is remarkable that the gait converged to the steady motion at high speed. The limit cycle stability in this case is, however, not obvious and we should investigate the mechanism in more detail.

Fig. 7 shows the simulation results where the slope is 0.30 [rad], $r = 0.30$ [m] and $\eta = 0.20$ [N·m·s/rad]. The walker started from a certain initial condition. We can see that a stable limit cycle was successfully generated. Since the coordinate differs from the compass-like biped as previously mentioned, the behavior of angular positions is unfamiliar. Fig. 7 shows that the total mechanical energy monotonically decreases during the stance phases because of the viscous friction.

B. Swing-leg Retraction

Gait stability is one of the most important factors in the study of limit cycle walking. The authors proposed an approach to the stability analysis based on a recurrence formula of the kinetic energy just before impact [12].

Let K [J] be the kinetic energy of the passive walker. A symmetric rimless wheel has the following recurrence formula:

$$K^-[i+1] = \varepsilon K^-[i] + \Delta E, \tag{17}$$

where $\varepsilon = K^+/K^-$ [-] is the energy-loss coefficient and ΔE [J] is the restored mechanical energy [12]. In rimless wheel, ε and ΔE are kept constant and the generated gait thus converges to one-period stable limit cycle. In general limit cycle walkers, however, these are not kept constant and thus the limit cycle analysis becomes complicated. Especially, swing-leg retraction (SLR) strongly changes the value of ε. SLR is a phenomenon that the swing-leg moves backward just prior to impact [4] as shown in Fig. 8, and has a great influence on the gait efficiency and limit cycle stability [5][6][7][8].

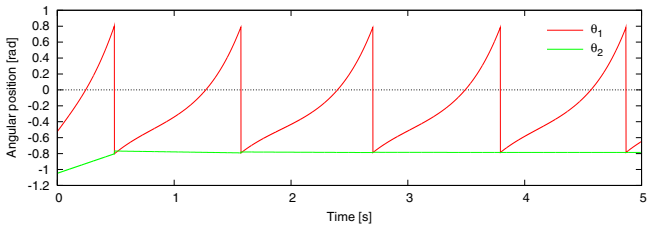

(a) Angular position

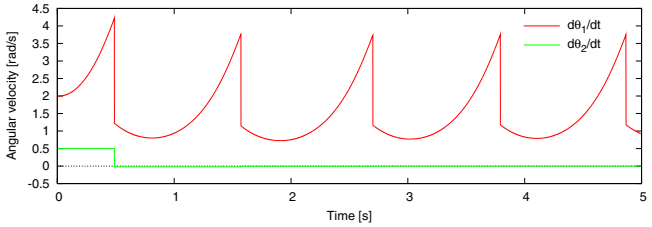

(b) Angular velocity

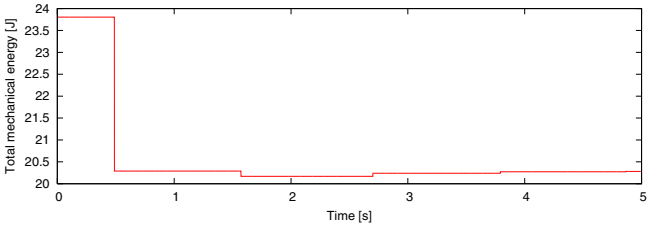

(c) Total mechanical energy

Fig. 6. Simulation results of passive-dynamic walking without viscous friction where slope is 0.30 [rad]

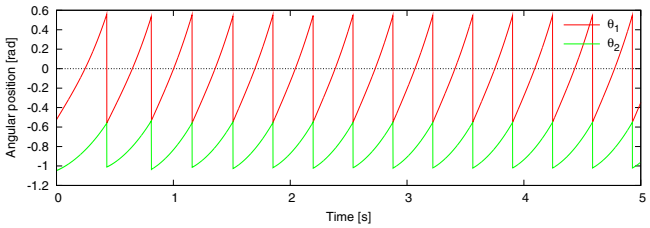

(a) Angular position

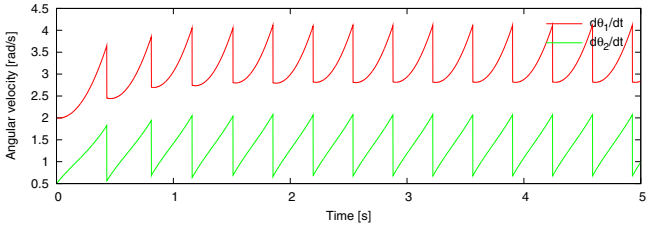

(b) Angular velocity

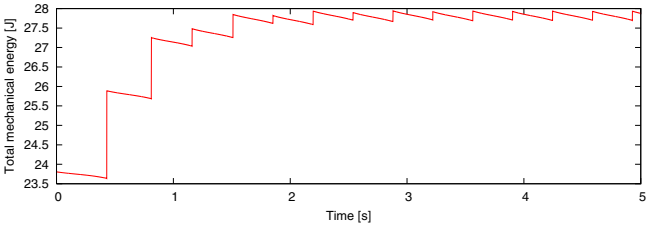

(c) Total mechanical energy

Fig. 7. Simulation results of passive-dynamic walking with viscous friction where slope is 0.30 [rad] and $\eta = 0.20$ [N·m·s/rad]

Let $\nu := \dot{\theta}_2^- / \dot{\theta}_1^-$ [-] be the ratio of angular velocity just before impact, then the angular velocity vector can be arranged as $\dot{\boldsymbol{\theta}}^- = \begin{bmatrix} 1 & \nu \end{bmatrix}^{\mathrm{T}} \dot{\theta}_1^-$. The kinetic energies just before and just after impact are also arranged as

$$K^- = \frac{1}{2} \begin{bmatrix} 1 \\ \nu \end{bmatrix}^{\mathrm{T}} \boldsymbol{M} \begin{bmatrix} 1 \\ \nu \end{bmatrix} \left(\dot{\theta}_1^- \right)^2, \tag{18}$$

$$K^+ = \frac{1}{2} \begin{bmatrix} 1 \\ \nu \end{bmatrix}^{\mathrm{T}} \boldsymbol{\Xi}^{\mathrm{T}} \boldsymbol{M} \boldsymbol{\Xi} \begin{bmatrix} 1 \\ \nu \end{bmatrix} \left(\dot{\theta}_1^- \right)^2. \tag{19}$$

The energy-loss coefficient is then rewritten as

$$\varepsilon = \frac{\begin{bmatrix} 1 \\ \nu \end{bmatrix}^{\mathrm{T}} \boldsymbol{\Xi}^{\mathrm{T}} \boldsymbol{M} \boldsymbol{\Xi} \begin{bmatrix} 1 \\ \nu \end{bmatrix}}{\begin{bmatrix} 1 \\ \nu \end{bmatrix}^{\mathrm{T}} \boldsymbol{M} \begin{bmatrix} 1 \\ \nu \end{bmatrix}} = \frac{N_\varepsilon}{D_\varepsilon}, \tag{20}$$

where

$$N_\varepsilon = I(I + I\nu^2 + 2ml^2) + 4ml^2 \cos(2\alpha)(I\nu + ml^2 \cos(2\alpha)), \tag{21}$$

$$D_\varepsilon = (I + 2ml^2)(I + I\nu^2 + 2ml^2). \tag{22}$$

This is a function of ν, but we also examine its property by changing the inertia moment, I.

ε is almost maximized regardless of the inertia moment around the zero swing-leg retraction ($\nu = 1.0$); the walker falls down as a one-link rigid body. Where $I = 0$, ε is kept constant and is $\cos^2(2\alpha)$. This result is identical to that of the rimless wheel and simplest walking model [8][12][13]. As reported in [8], ε is almost kept constant when $\nu < 1$ in the compass-like biped robot regardless of the mass distribution.

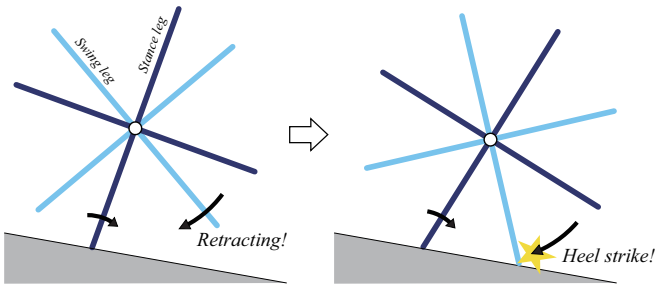

Fig. 8. Swing-leg retraction

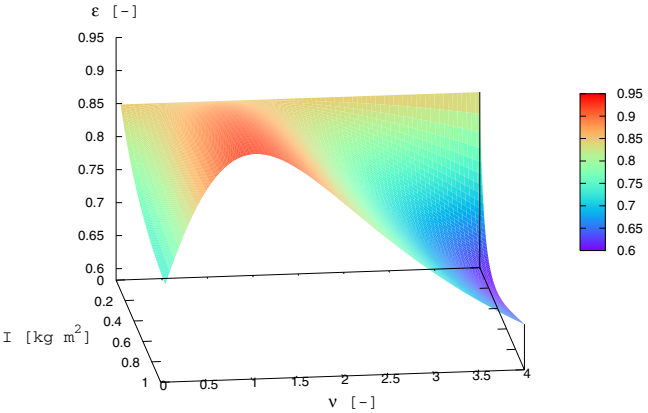

Fig. 9. 3D plot of energy-loss coefficient with respect to inertia moment and ratio of angular velocity

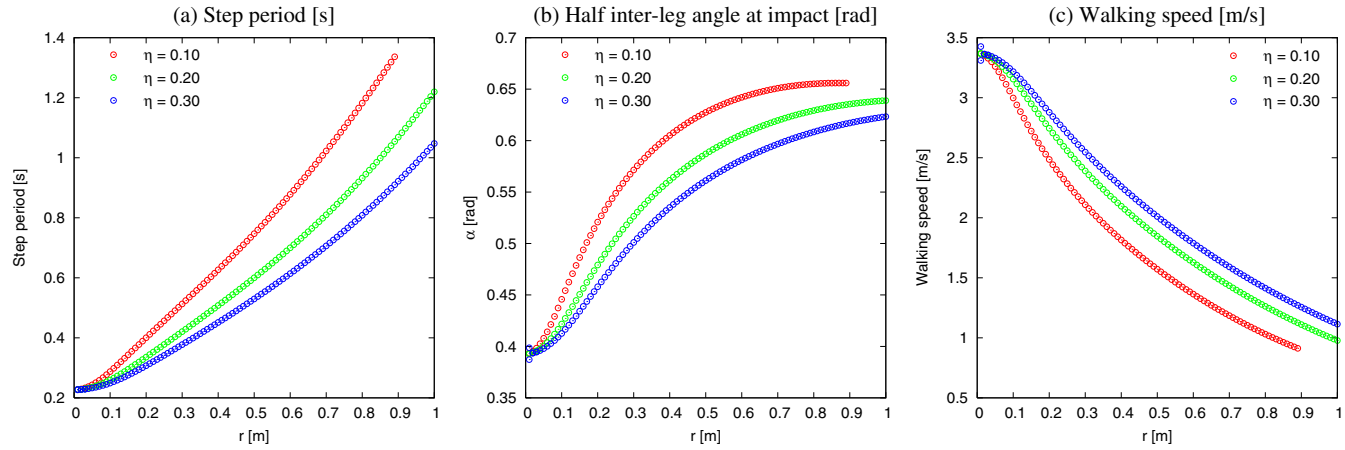

Fig. 10. Gait descriptors with respect to r for three values of η where slope is 0.30 [rad]

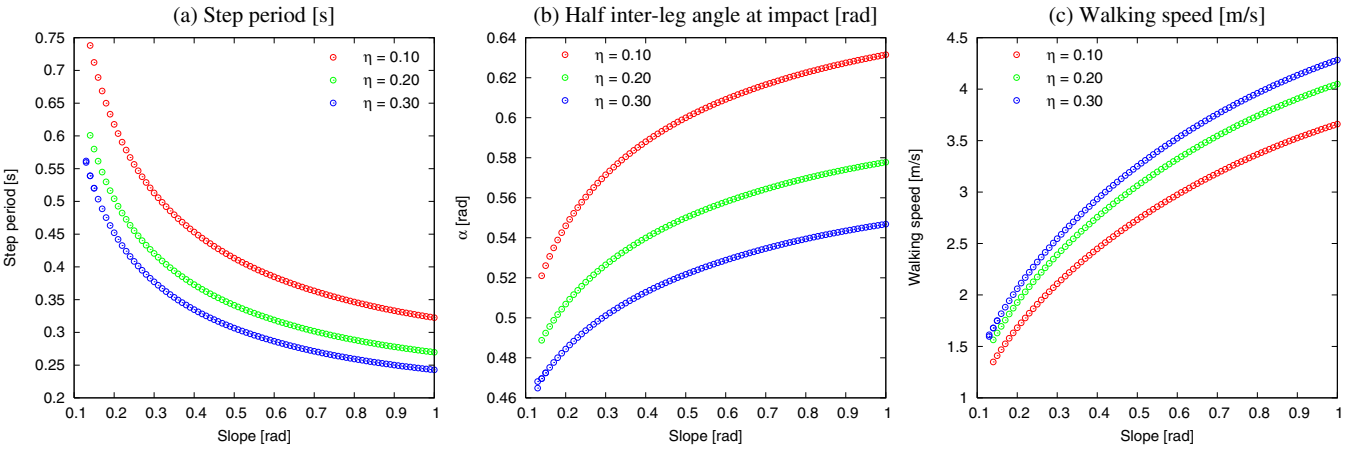

Fig. 11. Gait descriptors with respect to slope angle for three values of η where $r = 0.30$ [m]

In Fig. 9, however, ε is strongly affected when $\nu < 1$. This result comes from the difference of the walking models, but the essence is still unclear. We should investigate how ε changes with respect to the leg-mass position in the case of the compass-like biped.

In the passive-dynamic walker this paper considers, there is no possibility that the swing-leg frame rotate in a counterclockwise direction ($\nu > 0$), and it always rotates in a clockwise by the effect of viscous friction. It is sure that the condition $0 < \nu < 1$ holds in this model. From the plot in Fig. 9, ε is strongly affected by SLR when I is large, and the limit cycle stability is weak in this sense.

The effect of SLR in the presence of leg elasticity is also an interesting topic and is left as a future work.

C. Effect of Inertia Moment

We first analyze the effect of inertia moment by changing r $(0 < r \leq l = 1.0)$.

Fig. 10 shows the analysis results of the gait descriptors with respect to the radius, r, for three values of η. Here, (a) is the step period, (b) the half inter-leg angle at impact, α, and (c) the walking speed.

From (a), we can see that the step period monotonically increases as r increases in all cases. This is because the rotational motion becomes slower as the inertia moment increases, and this results in the larger half inter-leg angle as shown in (b). From (c), we can see that the walking speed monotonically decreases with respect to r. This is because the increasing rate of the step period is greater than that of the step length.

Where $\eta = 0.10$, a stable gait could not be generated when $r \geq 0.90$ [m]. This is because the walker cannot overcome the potential barrier at mid-stance. In other cases, stable gait generation was achieved. We should investigate the reason in the future. On the other hand, as r approaches zero, period-doubling bifurcation occurs.

D. Effect of Slope

Next, we analyze the change of the gait descriptors with respect to slope angle. Fig. 11 shows the results. In all cases, from (a), the step period monotonically decreases, and from (b), the step length monotonically increases as the slope increases. This is because the robot's overall motion becomes rapid, and the walking speed thus monotonically increases as the slope increases. In this range, period-doubling bifurcation

was not observed. Note that the walker without viscous friction can walk only on a steep slope because the step length or half inter-leg angle, α, is maximized in this case as shown in Fig. 6. Whereas in the presence of sufficient viscous friction it can walk on a gentle slope with a small step.

V. EXPERIMENTS

Now we are trying to achieve experimental dynamic walking (See Fig. 12). Generating a stable dynamic gait in the presence of viscous friction is not easy and successful walking for prolonged periods of time has not succeeded yet. There is a tendency that, even if the viscous friction exists, the walking motion does not continue for long period and converges to 1-period gait which is identical to that generated in the absence of viscous friction shown in Fig. 6. The gap between simulation and experiment comes from stiction, and the improvement is necessary.

We are also testing the effect of the telescopic-legged mode. The experimental results of passive-dynamic walking including double-support phase and running would be reported in our future papers.

VI. CONCLUSION AND FUTURE WORK

In this paper, we proposed a novel passive-dynamic walker and numerically analyzed its properties. In this walker, the swinging motion of the swing-leg frame was achieved by the viscosity at the central axis, or the stance leg only moves. The spoked walker has many possibilities for development of a novel robust and adaptive dynamic locomotion system. The following statements are left as future works to be investigated.

1) Actuation and control: It is interesting and necessary to add an actuator to the walker for generating a level dynamic gait. Controlling the swing-leg frame results in the angular momentum control. It enables the walker to create various motions. Combination with telescopic actuation of the stance leg is also an interesting topic. By extending the stance leg during stance phases, we can easily generate high-speed dynamic gait based on the asymmetric impact posture [11].

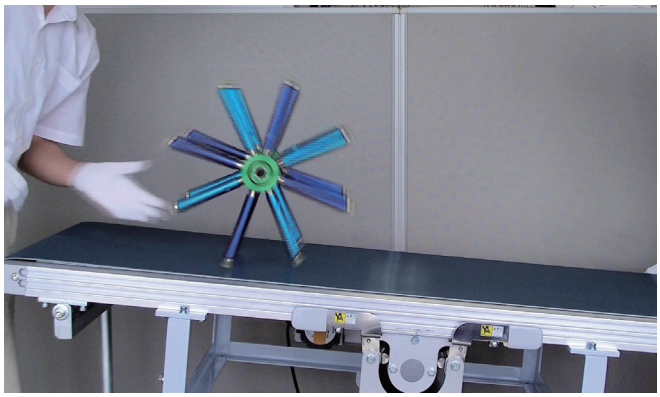

Fig. 12. Snapshot of walking experiment

2) Effect of leg elasticity: Now we are modeling the walker with leg springs and investigating the effect on the walking motion, gait efficiency, and stability. In this model, double-support phase would exist, and its utilization for stable gait generation is our main future subject.

3) Running: We are also trying to achieve passive-dynamic running on a steep slope. The results will be reported in a future paper.

VII. ACKNOWLEDGMENTS

The author withes to thank ONO-DENKI CO., LTD. for many helpful suggestions and technical supports in development of the prototype dynamic walker. The author also would like to thank Prof. Mizuhito Ogawa, Mr. Masashi Suguro, and Mr. Ryosuke Inoue, JAIST, for their helpful discussions and assistance for experiments.

REFERENCES

[1] T. McGeer, "Passive dynamic walking," *Int. J. of Robotics Research*, Vol. 9, No. 2, pp. 62–82, 1990.

[2] A. Goswami, B. Thuilot and B. Espiau, "Compass-like biped robot part I: Stability and bifurcation of passive gaits," *Research report, INRIA*, No. 2996, 1996.

[3] M. Garcia, A. Chatterjee and A. Ruina, "Speed, efficiency, and stability of small-slope 2D passive dynamic bipedal walking," *Proc. of the IEEE Int. Conf. on Robotics and Automation*, Vol. 3, pp. 2351–2356, 1998.

[4] A. Seyfarth, H. Geyer and H. Herr, "Swing-leg retraction: a simple control model for stable running," *J. of Experimental Biology*, Vol. 206, pp. 2547–2555, 2003.

[5] D. G. E. Hobbelen and M. Wisse, "Swing-leg retraction for limit cycle walkers improves disturbance rejection," *IEEE Trans. on Robotics*, Vol. 24, No. 2, pp. 377–389, 2008.

[6] M. Wisse, C. G. Atkeson and D. K. Kloimwieder, "Swing leg retraction helps biped walking stability," *Proc. of the IEEE-RAS Int. Conf. on Humanoid Robots*, pp. 295–300, 2005.

[7] F. Asano, "Robust pseudo virtual passive dynamic walking based on quasi-constraint on impact posture," *Proc. of the 9th Int. IFAC Symp. on Robot Control*, pp. 571–576, 2009.

[8] F. Asano, "Effects of swing-leg retraction and mass distribution on energy-loss coefficient in limit cycle walking," *Proc. of the IEEE/RSJ Int. Conf. on Intelligent Robots and Systems*, pp. 3214–3219, 2009.

[9] M. Coleman, A. Chatterjee and A. Ruina, "Motions of a rimless spoked wheel: A simple 3D system with impacts," *Dynamics and Stability of Systems*, Vol. 12, No. 3, pp. 139–160, 1997.

[10] J. B. Jeans and D. Hong, "IMPASS: Intelligent mobility platform with active spoke system," *Proc. of the IEEE Int. Conf. on Robotics and Automation*, pp. 1605–1606, 2009.

[11] F. Asano, "Dynamic gait generation based on asymmetric impact posture," *Proc. of the IEEE-RAS Int. Conf. on Humanoid Robots*, pp. 68–73, 2009.

[12] F. Asano and Z.W. Luo, "Asymptotically stable biped gait generation based on stability principle of rimless wheel," *Robotica*, Vol. 27, No. 6, pp. 949–958, 2009.

[13] M. Garcia, A. Chatterjee, A. Ruina and M. Coleman, "The simplest walking model: Stability, complexity, and scaling," *ASME J. of Biomechanical Engineering*, Vol. 120, No. 2, pp. 281–288, 1998.